Magnetic Resonance in Medicine 52:789–797 (2004)

# Defining a Local Arterial Input Function for Perfusion MRI Using Independent Component Analysis

Fernando Calamante,[1*] Morten Mørup,[2] and Lars Kai Hansen[2]

**Quantification of cerebral blood flow (CBF) using dynamic-susceptibility contrast MRI relies on the deconvolution of the arterial input function (AIF), which is commonly estimated from the signal changes in a major artery. However, it has been shown that the presence of bolus delay/dispersion between the artery and the tissue of interest can be a significant source of error. These effects could be minimized if a local AIF were used, although the measurement of a local AIF can be problematic. This work describes a new methodology to define a local AIF using independent component analysis (ICA). The methodology was tested on data from patients with various cerebrovascular abnormalities and compared to the conventional approach of using a global AIF. The new methodology produced higher CBF and shorter mean transit time values (compared to the global AIF case) in areas with distorted AIFs, suggesting that the effects of delay/dispersion are minimized. The minimization of these effects using the calculated local AIF should lead to a more accurate quantification of CBF, which can have important implications for diagnosis and management of patients with cerebral ischemia. Magn Reson Med 52:789–797, 2004. © 2004 Wiley-Liss, Inc.**

**Key words: perfusion; deconvolution; arterial input function; independent component analysis**

Dynamic susceptibility contrast (DSC) MRI is playing an increasingly important role in the diagnosis and management of acute stroke (1). It involves the intravenous injection of a bolus of a paramagnetic contrast agent and the rapid measurement of the changes in signal intensity during its passage through the brain (2). The signal intensity time changes can be converted to a concentration time curve $C(t)$, such that:

$$C(t) = \mathrm{CBF} \cdot (C_a(t) \otimes R(t)) \quad [1]$$

where CBF is the cerebral blood flow, $C_a(t)$ is the arterial input function (AIF), i.e., the concentration of contrast entering the tissue of interest at time $t$, $R(t)$ is the tissue residue function, i.e., the fraction of contrast agent concentration at time $t$ for the case of an ideal instantaneous bolus injected at $t = 0$, and the symbol $\otimes$ indicates the convolution operation (3).

Quantification of CBF relies on the deconvolution of the AIF to calculate the impulse response function $\mathrm{CBF} \cdot R(t)$, where the AIF is commonly estimated from the signal changes in a major artery. This estimated AIF is used as a *global* AIF for the whole slice. However, it has been shown that the presence of bolus delay and dispersion between the artery and the tissue of interest can be a significant source of error in CBF quantification (4–6), particularly in the presence of cerebrovascular abnormalities such as in patients with severe carotid stenosis and patients with moyamoya syndrome. These effects could be minimized if a *local* AIF (estimated from a smaller vessel closer to the tissue of interest) were used (7). However, measurement of a local AIF can be problematic due to, for example, partial volume effects (8,9).

Independent component analysis (ICA) can be used to identify temporal and/or spatial independent patterns, and it is based on the assumption that the signals of interest can be decomposed into a linear combination of statistical independent components (10). It has been widely used in MRI to study functional brain activity (11,12). It has also been used in DSC-MRI as a segmentation technique (13), and to remove the signal resulting from large vessels (14). The present work describes the use of ICA as a tool to define a local AIF, with the aim of minimizing the effects of bolus delay/dispersion and obtaining a more accurate quantification of CBF.

## MATERIALS AND METHODS

### Independent Component Analysis

ICA is a set of methods for blind signal separation sharing the assumption that the source signals are assumed statistically independent (see Ref. 12 for a recent review in the context of MRI). Blind signal separation refers to the common situation in signal processing in which we aim to separate unknown source signals from an unknown mixture. This happens, for example, in the so-called "cocktail party" problem where the target is to separate a number of simultaneous speakers based on one or more microphone measurements. In the case of DSC-MRI we are interested in separating the contribution of several signal sources: vascular components, tissue components, and a number of confounding sources, e.g., movements and parameter nonstationarity such as scanner "drift." These sources are characterized by being spatially segregated: Vascular components are spatially localized to vessels, while tissue components are located in gray and white matter, respectively. Movement leads to signals predominantly in high-contrast regions, i.e., at image "edges" orthogonal to the direction of motion, while scanner drift can lead to signals at image edges in general locations. Hence, we are interested in so-called spatial ICA in which the sources are spatially independent stochastic processes, sampled in unknown mixtures at different points in time. Formally

[1]Radiology and Physics Unit, Institute of Child Health, University College London, London, UK.

[2]Informatics and Mathematical Modelling, Technical University of Denmark, Lyngby, Denmark.

Grant sponsors: Wellcome Trust, Danish Technical Research Council, NHS Executive.

*Correspondence to: Fernando Calamante, PhD, Radiology and Physics Unit, Institute of Child Health, University College London, 30 Guilford Street, London WC1N 1EH, UK. E-mail: cfernan@ich.ucl.ac.uk

Received 20 January 2004; revised 7 April 2004; accepted 11 May 2004.

DOI 10.1002/mrm.20227

Published online in Wiley InterScience (www.interscience.wiley.com).

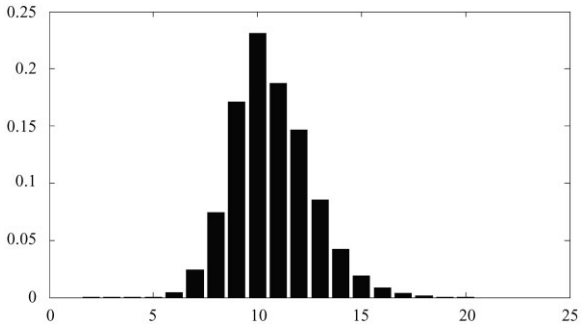


FIG. 1. Component probability distribution calculated using the Bayesian information criterion for the data acquired using GE-EPI on a patient with turbulence detected in MR angiography in the right middle, posterior, and anterior cerebral arteries. According to the histogram, the optimum number of independent components to describe this dataset is N = 10.

the measured mixture signal $C(x,t)$ will be assumed linear, hence, we assume that the source signal components at any given location ($x$) at a specific time instant ($t$) are simply added up without interference effects: $C(x,t) = \sum_{j=1}^{N} a_j(x) \cdot S_j(t) + \text{noise}$. Where $a_j(x)$ are the spatially independent source signals, while the mixing coefficients $S_j(t)$ quantify the levels of expression of signal sources $j$ at time $t$. An important complication that often arises in practical applications is that the number of sources ($N$) is unknown. Using a Bayesian ICA formulation this problem can be solved in the limit of many pixel locations ($x$) (15). The so-called Bayesian Information Criterion (BIC) selects the number of components by estimating the probability of the model containing $N$ sources given the observed data [$P(N|data)$], where the number of components is varied in a range [$0,N_{max}$], the signal variance not accounted for by the $N$ source components is assumed to be contributed by an additive normal independent identically distributed white noise signal component (the ICA Matlab code with BIC selection of the number of components is available from the web site http://isp.imm.dtu.dk/toolbox).

## Local AIF

The methodology to calculate the local AIF consists of the following steps:

1. The signal intensity time changes are converted to a concentration time curve $C(x,t)$ in each pixel (where $x$ denotes the spatial pixel position, and $t$ time).
2. The optimum number $N$ of independent components is estimated according to the BIC. This is illustrated in Fig. 1.
3. The calculated $C(x,t)$ is decomposed into the $N$ independent sources (and noise components, see Eq. 2). This is illustrated in Fig. 2 for the data from a patient where the optimum number of components is $N = 10$ (see Fig. 1).
4. The data are denoised to create $C_{tissue}(x,t)$ by removing the noise components:

$$C(x,t) = \sum_{j=1}^{N} a_j(x) \cdot S_j(t) + \text{noise} = C_{\text{tissue}}(x,t) + \text{noise}. \quad [2]$$

5. To determine the arterial contribution from the ICA, the components with clear nonarterial characteristics were discarded, i.e., those components representing tissue and/or venous flow (based on their spatial distribution and temporal characteristics, see, for example, the component $S_7(t)$ in Fig. 2), or components representing artifacts (based on their spatial distribution and temporal characteristics, see, for example, the component $S_8(t)$ in Fig. 2). For each of the remaining components (i.e., those with arterial contributions, subindexes labeled "arterial" in Eq. 3, below), a mask [$m_k(x)$] was defined with the voxels whose intensity was greater than a given threshold (the value of the threshold was determined interactively by the user for each component, such that the mask contained voxels consistent with the spatial distribution of arterial branches in the image). See Fig. 3a for an example of the masks created with the components with arterial contributions selected from those shown in Fig. 2. These contributions were combined to create $C_{art}(x,t)$ (see Fig. 3b):

$$C_{art}(x,t) = \sum_{\text{arterial}} m_k(x) \cdot a_k(x) \cdot S_k(t). \quad [3]$$

   Thresholding the map components to generate the masks has two purposes. First, to select only the voxels with significant contribution in the components that have a clear arterial spatial distribution (cf. z-scores in ICA of fMRI data (11)). In the absence of this threshold, even pixels with almost negligible intensity in the map component could have an important contribution to the final local AIF, since the resulting $C_{art}(x,t)$ dataset will be scaled to have uniform area under the peak (see step 6, below). Second, to aid the isolation of arterial component from tissue components in cases when these were not fully separated by the ICA (cf. tissue segmentation using ICA and thresholding (13)). Note that by using the masks, the $C_{art}(x,t)$ is defined only in some of the voxels (see Fig. 3b).
6. The $C_{art}(x,t)$ dataset is scaled to have the same area under the peak throughout the slice. This is based on the assumption that the integral under the arterial concentration has the same value for all tissues in the brain (16).
7. In some cases the thresholding approach described in step 5 left some delayed arterial components mixed with venous components. When present, this was most commonly observed with the sagittal sinus. This is illustrated in Fig. 4 for the data acquired on a patient with sickle-cell disease and left internal carotid artery occlusion: the very delayed arterial contribution in this patient (open arrow) is mixed with a

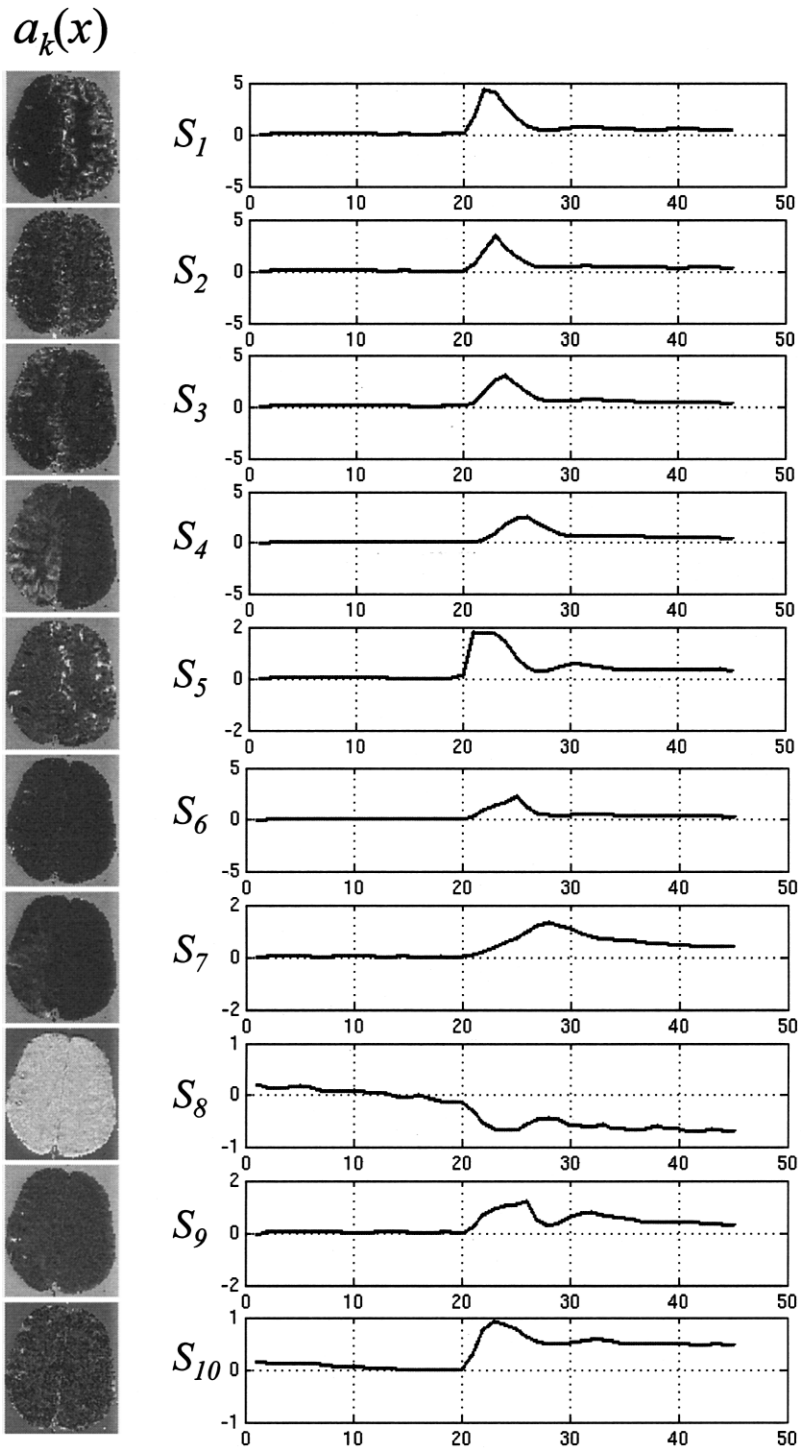


FIG. 2. ICA of the data acquired using GE-EPI on a patient with turbulence detected in MR angiography in the right middle, posterior, and anterior cerebral arteries. The figure shows the 10 independent spatial component maps on the left column, and the corresponding temporal components on the right column. The data correspond to the same patient as that shown in Fig. 1. The horizontal axes in the graphs display the image number (TR = 1.5 sec) corresponding to the 67.5 sec total acquisition time.

contribution from the sagittal sinus (filled arrow). Since the venous signal has higher signal intensity than the arterial component, it is not removed by the thresholding step 5. To eliminate this contribution to the $C_{art}(x,t)$ data, any residual venous contribution is interactively removed by manually drawing a region around the vein of interest and excluding these data from $C_{art}(x,t)$.

8. The AIF in the pixels where $C_{art}(x,t)$ is not defined (whose position is labeled $x_j$ in Eq. 4, below) is calculated from the remaining surrounding pixels (labeled $x_i$ in Eq. 4) according to their distance to the pixel of interest ($d_{ij}$), using a Gaussian-weighting factor:

$$C_{art}(x_j,t) = \frac{\sum_i w(d_{ij}) C_{art}(x_i,t)}{\sum_i w(d_{ij})}, \qquad [4]$$

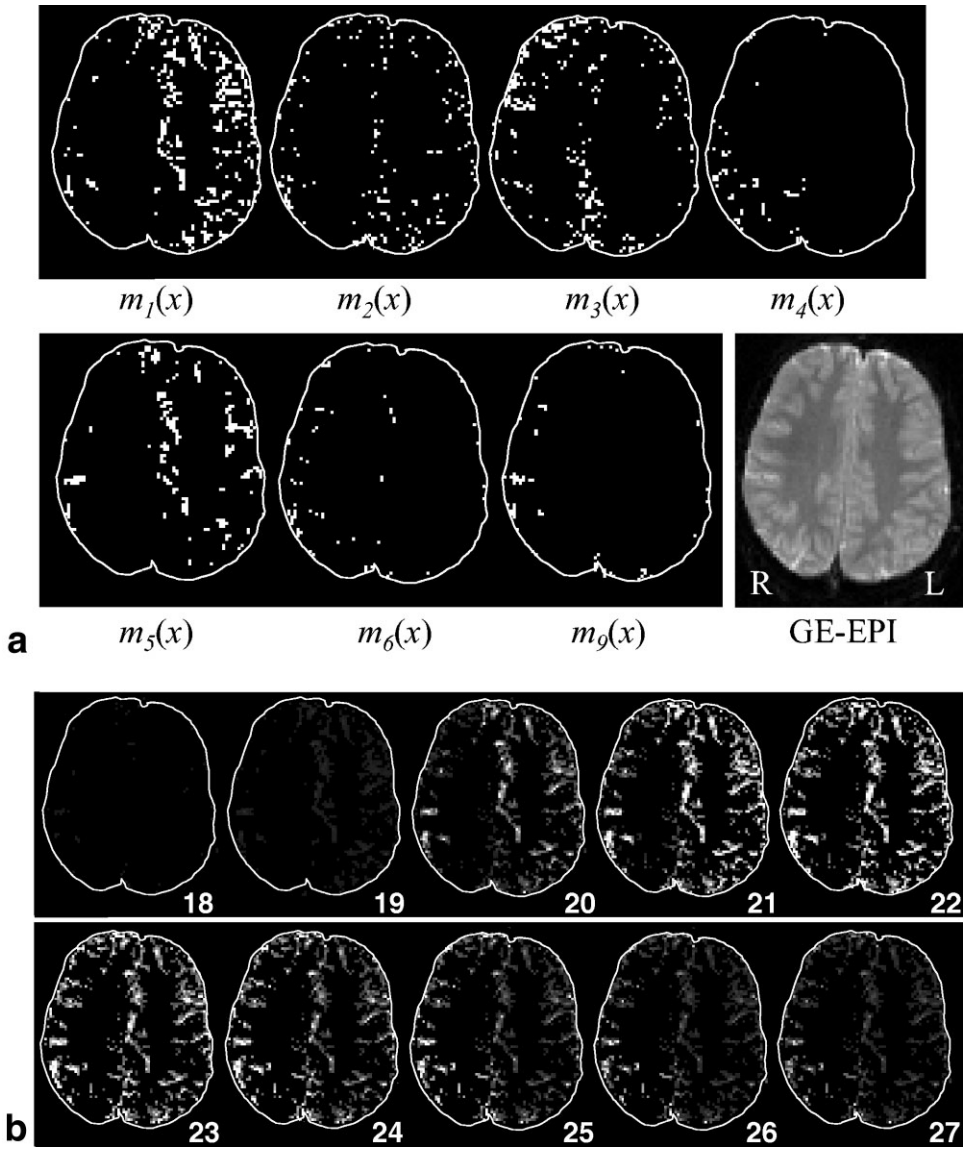


FIG. 3. **a:** Masks [$m_k(x)$] representing the voxels with arterial contributions in the data from the same patient as that shown in Fig. 2 (component numbers 1, 2, 3, 4, 5, 6, and 9). The figure in the bottom right is a $T_2^*$-weighted anatomical image. The data from the voxels in the masks were combined to create $C_{art}(x,t)$ as shown in Eq. 3. A set of 10 images (during the passage of the bolus) of the calculated $C_{art}(x,t)$ dataset is shown in **b**. The numbers inside each image correspond to the acquisition image order.

where the Gaussian-weighting factor (with standard deviation σ) is given by:

$$w(d_{ij}) = exp\left(-\frac{d_{ij}^2}{2\sigma^2}\right). \quad [5]$$

For the present study, a 10-pixel σ was empirically chosen (based on the gap size typically generated by the masks in step 5), and the Gaussian-weighting was truncated to a box of 30 × 30 pixels to avoid nonlocal contributions.

9. The resulting dataset is smoothed (with a 3 × 3 uniform kernel) to improve the signal-to-noise ratio (SNR); this smoothed dataset represents the *local AIF*. This is illustrated in Fig. 5.

### Patient Data

The methodology was tested on data obtained from patients with various cerebrovascular abnormalities. Data were acquired using either a gradient-echo (GE) echo-planar imaging (EPI) sequence (on a 1.5 T Siemens Symphony scanner, Siemens, Erlangen, Germany) or a spin-echo (SE) EPI sequence (on a 1.5 T Siemens Vision scanner). For the EPI acquisition, a multislice sequence was used (GE: TE/TR = 47/1500 ms, 12 slices; SE: TE/TR = 100/1500 ms, 6 slices), and a bolus of 0.15 mmol/kg body weight contrast agent (Gd-DTPA; Magnevist, Schering, Germany) was injected using an MR-compatible power injector (Medrad, Pittsburgh, PA).

### Deconvolution

To assess the effect of using a local AIF in the quantification of DSC-MRI, the data were analyzed in two different ways. First, $C_{tissue}(t)$ was deconvolved on a pixel-by-pixel basis using the local AIF generated in step 9, above. Second, the same $C_{tissue}(t)$ dataset was deconvolved using a global AIF. The global AIF was calculated from pixels manually selected (with an early, large signal drop) in a major artery (typically the middle cerebral artery) on the

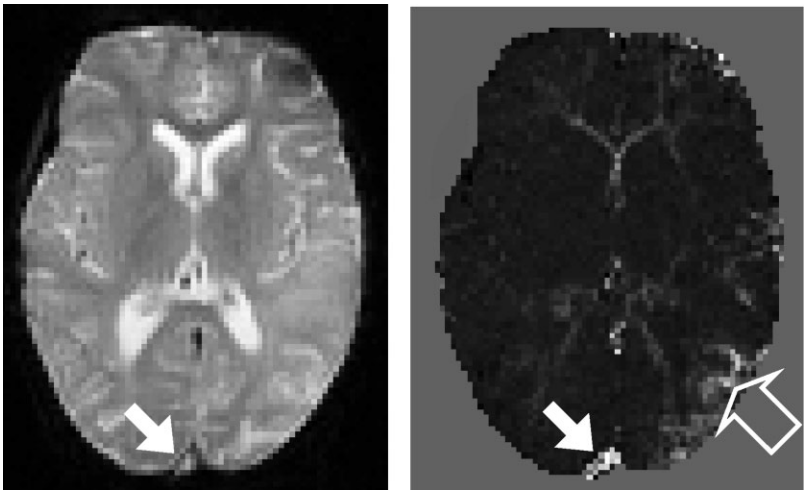

FIG. 4. $T_2^*$-weighted anatomical image (left) from a patient with sickle-cell disease and left internal carotid artery occlusion. The image on the right shows one of the spatial components obtained by ICA. A mixture of very delayed arterial contribution (open arrow) and venous contribution (filled arrows) is present in this spatial component.

contralateral hemisphere. Deconvolution was performed using singular value decomposition (SVD) (3), but with a reduced threshold (5% (17)) for the truncation of the SVD expansion, due to the improved SNR after signal denoising using ICA (see step 4, above). A $3 \times 3$ uniform smoothing was applied before deconvolution to further improve the SNR. CBF maps were calculated from the maximum of the corresponding impulse response function (3). Cerebral blood volume (CBV) maps were calculated from the area under $C_{tissue}(t)$ (normalized to the area under the corresponding AIF (2)). To calculate the area, the contribution from the recirculation was removed by fitting the concentration time curves to a gamma-variate function (2). Finally, mean transit time (MTT) maps were calculated by the central volume theorem as the ratio CBV/CBF (2).

## RESULTS

### Optimum Number of Independent Components

The optimum number of components depended on the type of sequence (GE vs. SE) and on the degree of vascular abnormalities in the patients (the more heterogeneity in the temporal characteristics of the vascular supply to the slice, the more the number of components). The optimum number was smaller for SE (typically 3–5 components for the patients investigated) than for GE (typically 8–13 components). It should be noted that this is not due to a difference in the degree of vascular abnormalities in the patients studied with each sequence (for example, both cases included data from patients with moyamoya syndrome).

### Local AIF

The identification of arterial contribution in the components (see step 5, above) was much easier in the datasets acquired using GE-EPI than in those acquired using SE-EPI. The separation between arterial and tissue contributions was more marked in the data acquired using GE-EPI, while only a relatively small number of components included arterial contributions (typically 1–3 components) for the SE-EPI case, and these were usually more mixed with tissue component than for the GE-EPI case (data not shown).

The ICA approach defined a local AIF that was heterogeneous in all the patients studied, with some areas displaying delayed, wider peaks, consistent with the patients' vascular abnormality. This is illustrated in Fig. 5 for the data acquired using GE-EPI. This figure show the local AIF calculated for the data from a patient with MR angiography turbulence in the right middle, posterior, and anterior cerebral arteries (Fig. 5a), and from a patient with sickle-cell disease with left internal carotid artery occlusion (Fig. 5b). Similar results were obtained using SE-EPI (see, for example, Fig. 6a for the data from a patient with right internal carotid artery stenosis, and Fig. 6b for a patient with bilateral moyamoya syndrome).

To investigate the sensitivity of the calculated local AIF to the particular choice of the optimum number of components, the analysis of the data from the patient shown in Figs. 2, 3, and 5 was repeated assuming a nonoptimum number of components (15 components were used, cf. optimum number 10 found using the BIC). Although small differences were observed in some of the components, and some extra components related to artifacts were identified, the use of the nonoptimum number of components did not have a noticeable effect on the final local AIF (data not shown).

### Deconvolution Analysis

The effect of defining a local AIF on the analysis of DSC-MRI data was assessed by performing the deconvolution using either the local AIF or a global AIF (currently the common practice method). Various differences were observed when comparing the maps depending on the AIF used, in particular CBF underestimation and MTT overestimation when the global AIF was used. This is illustrated in Fig. 7 for two GE-EPI cases and two SE-EPI cases. (Note: the CBV maps for the two methods are not shown because they are equivalent (up to a scaling factor, since the local AIF is normalized to have uniform area)).

To quantify the effect of AIF choice, the mean values of CBF were measured in gray matter regions manually

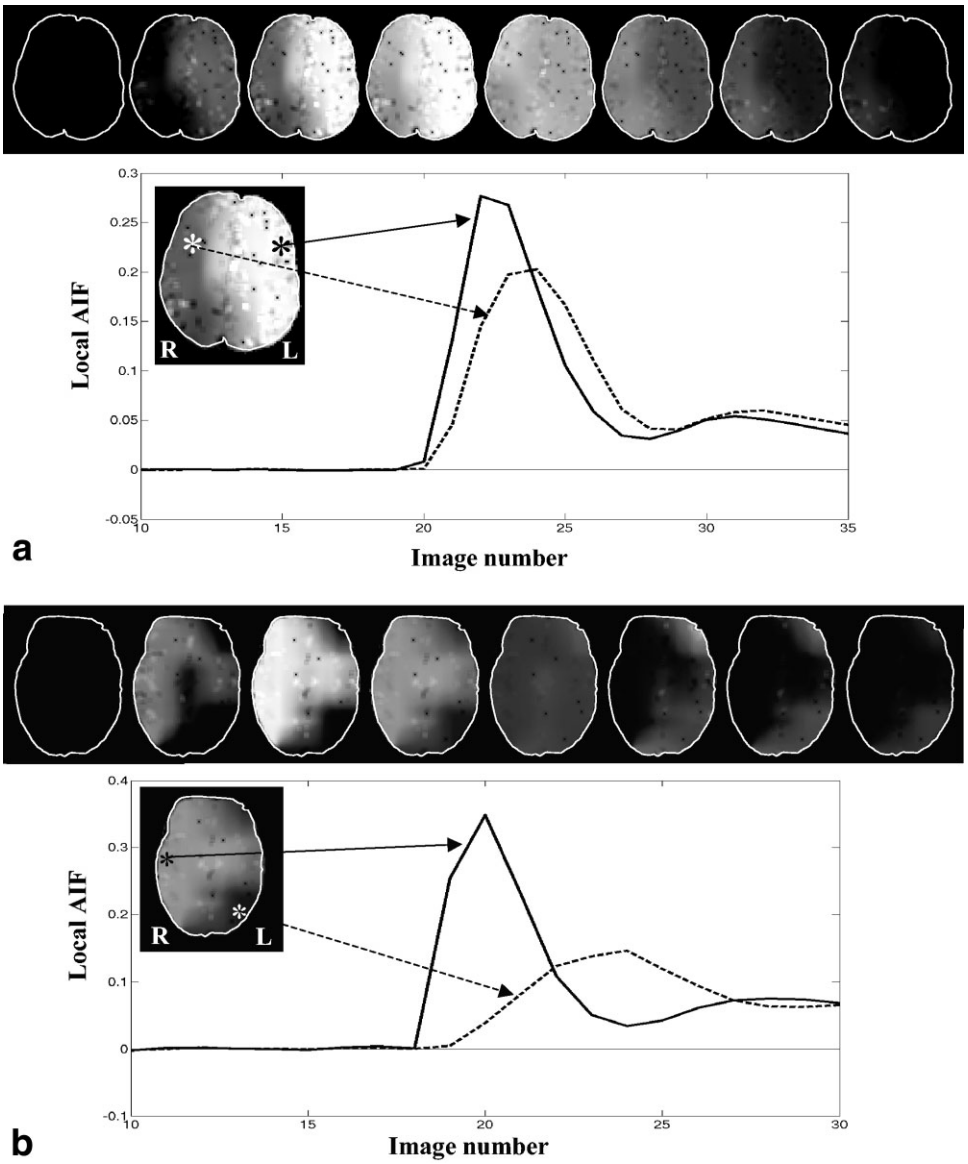


FIG. 5. Local AIF defined from data acquired using GE-EPI on (**a**) a patient with turbulence detected in MR angiography in the right middle, posterior, and anterior cerebral arteries (same patient as that shown in Fig. 3), and on (**b**) a patient with sickle-cell disease with left internal carotid artery occlusion. Each figure shows a set of eight images during the passage of the bolus of the local AIF (top), and a graph with the local AIF (in arbitrary units) for two gray matter pixels (bottom). The solid line corresponds to the local AIF from a pixel in normal-appearing gray matter (shown by the black asterisk in the inset figure). The dashed line the corresponding local AIF from a pixel in abnormal grey matter (shown by the white asterisk).

drawn in the areas marked with arrows in Fig. 7. The values were normalized to the corresponding mean values from a similar region in the contralateral side. For the cases shown in Fig. 7 acquired using GE-EPI, the ipsilateral/contralateral CBF ratios were increased using the local AIF from ~0.3 to 0.55 (top row), from 0.5 to 1.0 and 0.3 to 1.1 for the anterior and posterior regions, respectively (second row). Similarly, for the cases acquired using SE-EPI, the CBF ratios were increased from ~0.4 to 0.7 (third row), from 0.5 to 0.7 (bottom row).

## DISCUSSION

A new methodology to define a local AIF was presented. The methodology is based on the decomposition of the concentration time data on linearly independent components, and the use of thresholding of these components to identify arterial contributions, which are then combined to define a local AIF. The methodology was tested on data from patients with various cerebrovascular abnormalities. The local AIF generated in these patients was found to display regional heterogeneity, with areas with bolus arrival delay and wider peaks, which were consistent with the patients' vascular abnormalities.

To assess the effect on perfusion quantification, the maps calculated using deconvolution of the local AIF were compared to the corresponding maps calculated using the conventional approach (based on a global AIF). The new methodology produced higher CBF and shorter MTT (compared to the global AIF case) in the regions where the local AIF was distorted. In some cases, the abnormalities detected using the global AIF were in fact completely eliminated in the maps calculated using the local AIF information. Since the presence of bolus delay and/or dispersion has been shown to introduce CBF underestimation and MTT overestimation (4–6), the present results suggest that these effects are significantly minimized. Therefore, although the true perfusion values are not known in the patients included in this study, the use of the local AIF should lead, in principle, to a more accurate quantification

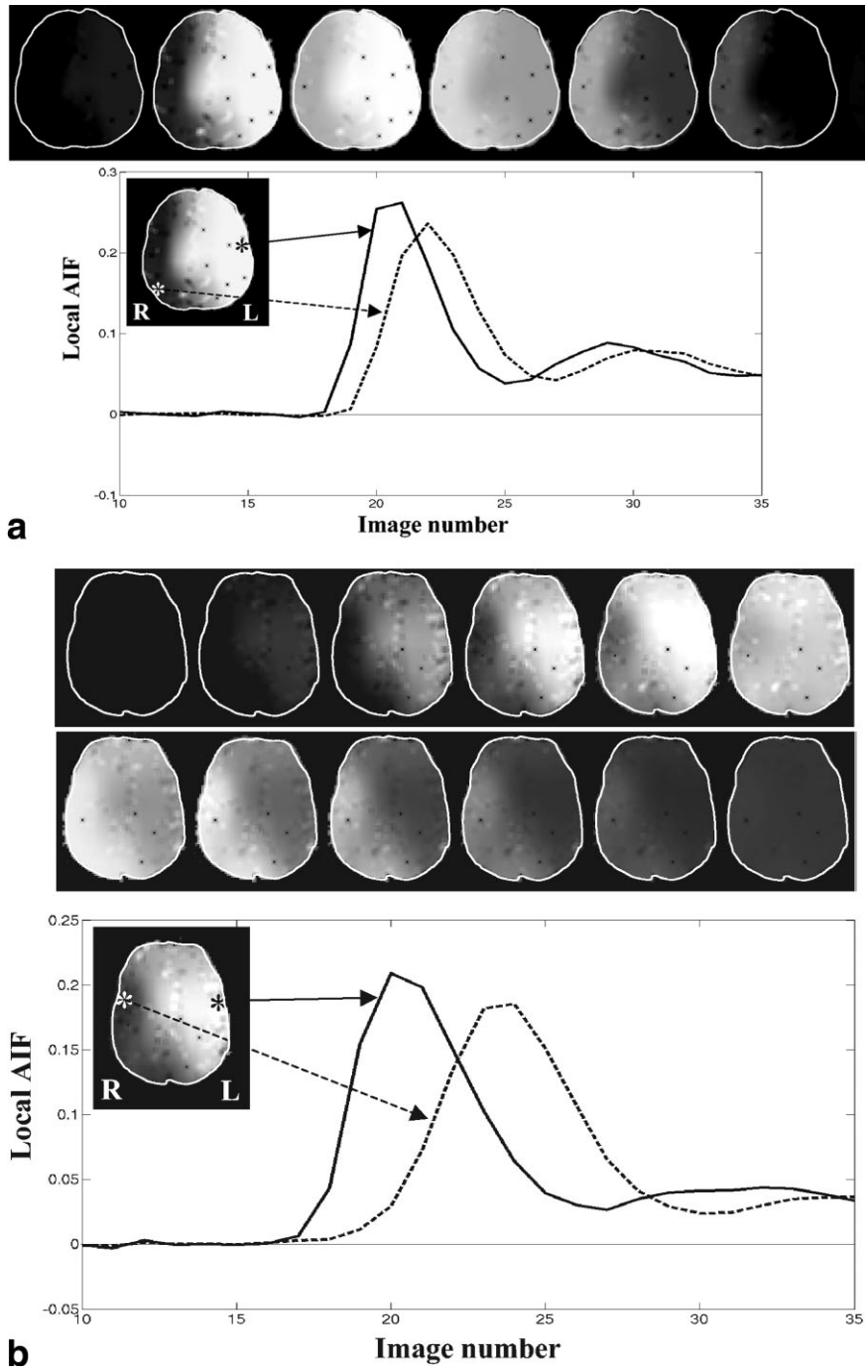


FIG. 6. Local AIF defined from data acquired using SE-EPI on a patient with right internal carotid artery stenosis (**a**), and on a patient with bilateral moyamoya syndrome (the MR scan was performed after surgical revascularization to the left hemisphere) (**b**). Each figure shows a set of images during the passage of the bolus (six in **a** and 12 in **b**) of the local AIF (top), and a graph with the local AIF (in arbitrary units) for two gray matter pixels (bottom). The solid line corresponds to the local AIF from a pixel in normal-appearing grey matter (shown by the black asterisk in the inset figure). The dashed line the corresponding local AIF from a pixel in abnormal gray matter (shown by the white asterisk).

of perfusion. This can have important implications for the diagnosis and management of patients with cerebral ischemia. Recent studies have focused on improving the characterization of the mismatch area between the diffusion and perfusion abnormalities, with the aim of differentiating tissue that will eventually infarct from tissue that will remain viable (see, for example, Refs. 18, 19). As shown in this study, the use of a local AIF can greatly influence the CBF and MTT values in areas with distorted AIF, which can potentially modify the tissue outcome classification. Despite the several methods for tissue classification currently available, their sensitivity/specificity values remain limited. This might hinder the widespread use of MRI as a tool for the identification of suitable patients for treatment (e.g., thrombolysis in acute stroke). Therefore, future studies should assess the effect of defining a local AIF on the sensitivity/specificity of tissue classification models.

It should be noted that the resulting AIF in the voxels identified by the masks (step 5) is different from the one that would have been obtained by directly thresholding the original data (equivalent to keeping *all* the components). Since the masks are not completely overlapping, each pixel will have some of the components that will not contribute to the expansion in Eq. 3. The logic behind this

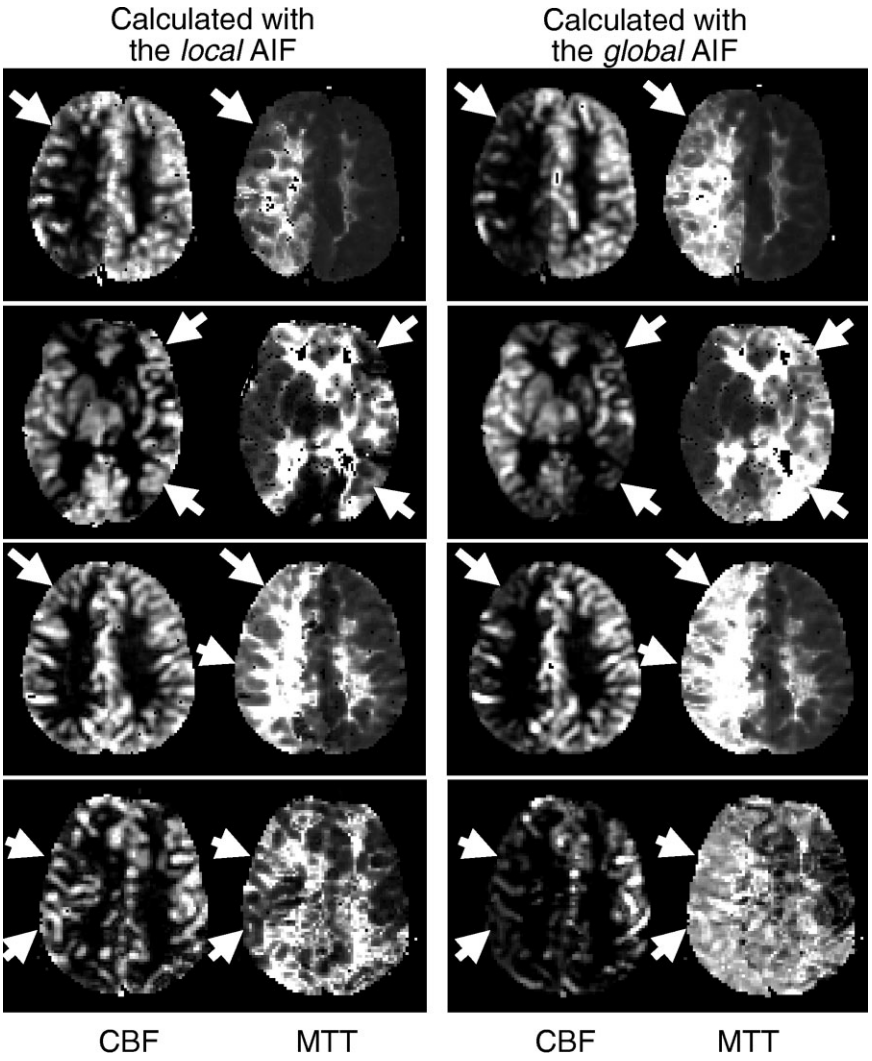


FIG. 7. Maps obtained with deconvolution analysis using the local AIF (left pair) and the global AIF (right pair). Each pair shows the CBF map (left) and the MTT map (right). The figure shows the results for the data acquired with GE-EPI (top 2) and SE-EPI (bottom 2) on four different patients (from top to bottom): i) patient with turbulence detected in MR angiography in the right middle, posterior, and anterior cerebral arteries (same patient as that shown in Fig. 5a); ii) patient with sickle-cell disease (same patient as that shown in Fig. 5b); iii) patient with right internal carotid artery stenosis (same patient as that shown in Fig. 6a); iv) patient with bilateral moyamoya syndrome (same patient as that shown in Fig. 6b). Various differences can be seen when comparing the maps depending on the AIF used, in particular CBF underestimation and MTT overestimation when the global AIF was used (see arrows).

approach is that the components left out are believed to be associated with tissue/venous/artifact contributions. Therefore, ICA provides a method to separate the concentration in components, and the methodology presented here a "recipe" to select some of those components.

Certain differences were found when applying the methodology to data acquired using GE-EPI and SE-EPI. For example, a larger number of optimum components were detected in the GE-EPI data, and the separation of arterial from tissue contributions in these components was much easier. These findings are related to the different vessel size sensitivity of these MR sequences. It has been shown that susceptibility contrast in GE images arises from both large and small vessels, whereas in SE images it is dominated by the small, capillary-size vessels (20). Therefore, the identification of the vascular signal is much simpler using a $T_2$*-weighted sequence. Moreover, it could have been expected that extracting local AIF information from SE data is not possible. However, it should be noted that the SE used in this study is based on an EPI acquisition, and it has therefore a degree of $T_2$* weighting (21).

Although the methodology defines an AIF for each pixel, in some areas this is done indirectly using the neighboring information (see steps 8 and 9). This is unavoidable, since there will always be regions in the image where the arterial information is very limited (e.g., some white matter areas). The approach used in this work in based on the assumption of AIF similarity between neighboring voxels. The validity of this assumption may be questioned in some cases, and an alternative method could be used. Although, in principle, the distribution of the arterial territories could be used as an improvement, large intersubject variability has been observed (22), which could introduce further errors.

It should be mentioned that the current implementation of the method to define a local AIF is based on a semi-manual approach. For example, user input is required in step 5 (to chose the threshold to define masks for each spatial component) and step 7 (to remove any residual venous contribution). We are currently working on a more automated approach.

One of the main limitations of any method that defines a local AIF is its validation. Although the defined local AIF agrees well with the global AIF in the voxels filled primarily with vessels (data not shown), in the general case it is not possible to validate the accuracy of the defined local AIF directly due to the lack of a gold standard. Numerical simulations may provide some validation, but they need to

be carefully designed to reflect a realistic representation of the partial volume effects and signal changes that are present in real cases. Alternatively, the local AIF can be validated indirectly by assessing the accuracy of the perfusion maps. This also is not straightforward, since the deconvolution process will introduce errors, which must be distinguished from those associated with the local AIF. Furthermore, perfusion must also be measured using a gold standard to compare with the results obtained using MRI. Due to these difficulties, an alternative (and probably more realistic) approach is to assess its effect on practical applications rather than to attempt a validation of the methodology. For example, as mentioned before, the effect of using a local AIF on the sensitivity/specificity of predictive models of tissue infarction could be investigated. If these are improved, the use of the local AIF is justified, even though the AIF information might not be strictly correct.

In summary, a new methodology to define a local AIF using ICA was described and compared to the conventional approach of using a global AIF. The new methodology produced higher CBF and shorter MTT (compared to the global AIF case) in areas with distorted AIFs, suggesting that the effects of delay/dispersion are minimized. The minimization of these effects should lead to a more accurate quantification of perfusion, which can have important implications for diagnosis and management of patients with cerebral ischemia. A further advantage of the proposed methodology is the improved SNR due to the denoising capabilities of the ICA, which should further contribute to improve the accuracy of DSC-MRI quantification.

## REFERENCES


1. Schellinger PD, Fiebach JB, Hacke W. Imaging-based decision making in thrombolytic therapy for ischemic stroke: present status. Stroke 2003;34:575–583.
2. Calamante F, Thomas DL, Pell GS, Wiersma J, Turner R. Measuring cerebral blood flow using magnetic resonance techniques. J Cereb Blood Flow Metab 1999;19:701–735.
3. Østergaard L, Weisskoff RM, Chesler DA, Gyldensted C, Rosen BR. High resolution measurement of cerebral blood flow using intravascular tracer bolus passages. I. Mathematical approach and statistical analysis. Magn Reson Med 1996;36:715–725.
4. Calamante F, Gadian DG, Connelly A. Delay and dispersion effects in dynamic susceptibility contrast MRI: simulations using singular value decomposition. Magn Reson Med 2000;44:466–473.
5. Calamante F, Yim PJ, Cebral JR. Estimation of bolus dispersion effects in perfusion MRI using image-based computational fluid dynamics. NeuroImage 2003;19:341–353.
6. Wu O, Østergaard L, Koroshetz WJ, Schwamm LH, O'Donnell JO, Schaefer PW, Rosen BR, Weisskoff RM, Sorensen AG. Effects of tracer arrival time on flow estimates in MR perfusion-weighted imaging. Magn Reson Med 2003;50:856–864.
7. Alsop D, Wedmid A, Schlaug G. Defining a local input function for perfusion quantification with bolus contrast MRI. In: Proc 10th Annual Meeting ISMRM, Honolulu, 2002. p 659.
8. van Osch MJP, Vonken EPA, Bakker CJG, Viergever MA. Correcting partial volume artifacts of the arterial input function in quantitative cerebral perfusion MRI. Magn Reson Med 2001;45:477–485.
9. Lin W, Celik A, Derdeyn C, An H, Lee Y, Videen T, Østergaard L, Powers WJ. Quantitative measurements of cerebral blood flow in patients with unilateral carotid artery occlusion: a PET and MR study. J Magn Reson Imag 2001;14:659–667.
10. Hyvärinen A, Oja E. Independent component analysis: algorithms and applications. Neural Networks 2000;13:411–430.
11. McKeown MJ, Makeig S, Brown GG, Jung T-P, Kindermann SS, Bell AJ, Sejnowski TJ. Analysis of fMRI data by blind separation into independent spatial components. Hum Brain Mapp 1998;6:160–188.
12. McKeown MJ, Hansen LK, Sejnowski TJ. Independent component analysis of functional MRI: What is signal and what is noise? Curr Opin Neurobiol 2003;13:620–629.
13. Kao Y-H, Guo W-Y, Wu Y-T, Liu K-C, Chai W-Y, Lin C-Y, Hwang Y-S, Liou AJ-K, Wu H-M, Cheng H-C, Yeh T-C, Hsieh J-C, Teng MM-H. Hemodynamic segmentation of MR brain perfusion images using independent component analysis, thresholding, and Bayesian estimation. Magn Reson Med 2003;49:885–894.
14. Carroll TJ, Haughton VM, Rowley HA, Cordes D. Confounding effect of large vessels on MR perfusion images analyzed with independent component analysis. AJNR Am J Neuroradiol 2002;23:1007–1012.
15. Kolenda T, Hansen LK, Larsen J. Signal detection using ICA: application to chat room topic spotting. In: Proc ICA, San Diego, 2001. p 540–545.
16. Axel L. Cerebral blood flow determination by rapid-sequence computed tomography. Radiology 1980;137:676–686.
17. Murase K, Shinohara M, Yamazaki Y. Accuracy of deconvolution analysis based on singular value decomposition for quantification of cerebral blood flow using dynamic susceptibility contrast-enhanced magnetic resonance imaging. Phys Med Biol 2001;46:3147–3159.
18. Butcher K, Parsons M, Baird T, Barber A, Donnan G, Desmond P, Tress B, Davis S. Perfusion thresholds in acute stroke thrombolysis. Stroke 2003;34:2159–2164.
19. Shih LC, Saver JL, Alger JR, Starkman S, Leary MC, Vinuela F, Duckwiler G, Gobin YP, Jahan R, Villablanca JP, Vespa PM, Kidwell CS. Perfusion-weighted magnetic resonance imaging thresholds identifying core, irreversibly infarcted tissue. Stroke 2003;34:1425–1430.
20. Weisskoff RM, Zuo CS, Boxerman JL, Rosen BR. Microscopic susceptibility variation and transverse relaxation. Theory and experiment. Magn Reson Med 1994;31:601–610.
21. Birn RM, Bandettini PA. The effect of T2' changes on spin-echo EPI-derived brain activation maps. In: Proc 10th Annual Meeting ISMRM, Honolulu, 2002. p 1324.
22. van der Zwan A, Hillen B. Review of the variability of the territories of the major cerebral arteries. Stroke 1991;22:1078–1084.